Journal of Structural Geology, Vol. 8, No. 1, pp. 15 to 33, 1986
Printed in Great Britain

0191-8141/86 $03.00 + 0.00

Structures and fabrics in a crustal-scale shear zone, Betic Cordillera, SE Spain

J. P. PLATT and J. H. BEHRMANN*

Department of Earth Sciences, Oxford University, Parks Road, Oxford OX1 3PR, U.K.

(*Received* 8 *May* 1984; *accepted in revised form* 8 *March* 1985)

Abstract—A broad zone of dominantly ductile high-strain deformation lies beneath the Aguilón nappe in the Sierra Alhamilla, southern Spain. It forms part of a crustal-scale movement zone, traceable through much of the Betic Cordillera, which separates the Higher Betic Nappes from the underlying Nevado–Filabride Complex. The zone is characterized in outcrop by a distinctive platy foliation and a strong NNE-trending stretching lineation. Microstructural characteristics include quartz ribbons, mica fish, augen of feldspar and other minerals in a matrix of dynamically recrystallized quartz, and extensional crenulation cleavages. Narrow bands of ultramylonite and cataclasite occur within and on the margins of the movement zone. Deformation occurred under lower greenschist-facies conditions and was accompanied by retrogression of earlier higher-grade mineral assemblages.

Structures in the movement zone developed in a temporal sequence, beginning with isoclinal folding and transposition of older foliations. This was followed by the formation of extensional crenulation cleavages, and the progressive localization of strain into the ultramylonite bands. Mylonitic foliation in these bands is deformed by syn-mylonite folds restricted to the bands. All these structures were then deformed by S- to SE-vergent small-scale folds restricted to the movement zone as a whole. Cataclasis, associated with alteration, is localized along the ultramylonite bands and indicates a transition to late-stage brittle deformation. The lower boundary of the movement zone is gradational: strain decreases, recrystallized grainsize and the degree of recrystallization of quartz increases, and pressure solution becomes the dominant deformation mechanism in mica-schist.

Asymmetric quartz fabrics in the movement zone indicate a NNE sense of shear; but variations in the degree of asymmetry suggest that flow was partitioned, with the ultramylonite bands taking up much of the shear strain, and the intervening rocks deforming more slowly and with a lower degree of non-coaxiality. Diffuse fabrics in the fine-grained ultramylonite bands may indicate a switch to a grainsize-sensitive deformation mechanism, and an overall downward increase in the opening angle of crossed-girdle fabrics may reflect increased water activity at depth.

INTRODUCTION

THE BETIC Cordillera in southern Spain is the westernmost segment of the Alpine orogenic system in Europe, and was formed by the interaction of the European and African plates in Late Mesozoic and Early Tertiary time. The precise pattern of plate motions that led to mountain building is unclear, although it almost certainly involved dextral motion of Spain with respect to Africa as well as convergence (Dewey *et al.* 1973). Plate-tectonic analysis of the region is complicated by the fact that the orogen connects around the Gibraltar arc with the Rif (Didon *et al.* 1973), curving through nearly 180°. The existence of an Alboran microplate, whose independent motion relative to Africa and Spain created the present geometry, was suggested by Andrieux *et al.* (1971). One difficulty with any analysis in terms of plate motions, however, is the lack of a clearly identifiable plate boundary, or suture, in the Betic Cordillera. A possible candidate is the Sub-Betic Zone, which separates the pre-Betic foreland fold-belt in the northeast from the largely metamorphic Betic Zone in the south (Fig. 1). The central Sub-Betic contains a deep-water Mesozoic to Early Tertiary basinal sequence, associated with minor basaltic volcanics, and was apparently the locus of some degree of rifting in mid-Jurassic time (Hermes 1978). The zone has been affected by thrusting (García-Hernandez *et al.* 1980) and possibly by dextral wrench faulting (Hermes 1978). No discrete suture or fossil plate boundary can be identified within the zone, however.

An alternative possibility is that a suture is hidden within the Betic Zone proper. This consists of a pile of large-scale nappes, generally regarded as having been emplaced towards the north (Aldaya 1969, Egeler & Simon 1969, Torres-Roldán 1979), and this sense of movement has been confirmed by recent structural work (Platt 1982, Behrmann & Platt 1982). Torres-Roldán (1979) suggested that the Betic nappes could be divided into two broad groups distinguished by fundamentally different metamorphic histories. Some units in the lower group (Nevado–Filabride Complex) show an early high-pressure/low-temperature (glaucophane–schist-facies) metamorphism, followed by a later medium P/T ratio event. By contrast, some of the overlying nappes (Alpujarride and Malaguide Complexes, here referred to as the Higher Betic Nappes) show an evolution from medium to low P/T ratio metamorphism. Torres-Roldán suggested that these two groups originally formed a paired metamorphic belt, with the Nevado–Filabrides representing the subducted leading edge of the European plate, and the Higher Betic Nappes belonging to the overthrust African plate. The contact between the two may therefore be the suture, with a displacement of tens to hundreds of kilometres. It is commonly marked by a broad zone of ductile deformation, mylonite, and cataclasite, which was referred to as the Betic Movement Zone by Platt & Vissers (1980). We retain this term (BMZ for short) as it appears to follow the most important discrete tectonic contact in the Betic Cordillera,

* Present address: Institut für Geologie, Universitat Tübingen, Sigwartstrasse 10, D 7400 Tübingen, West Germany.

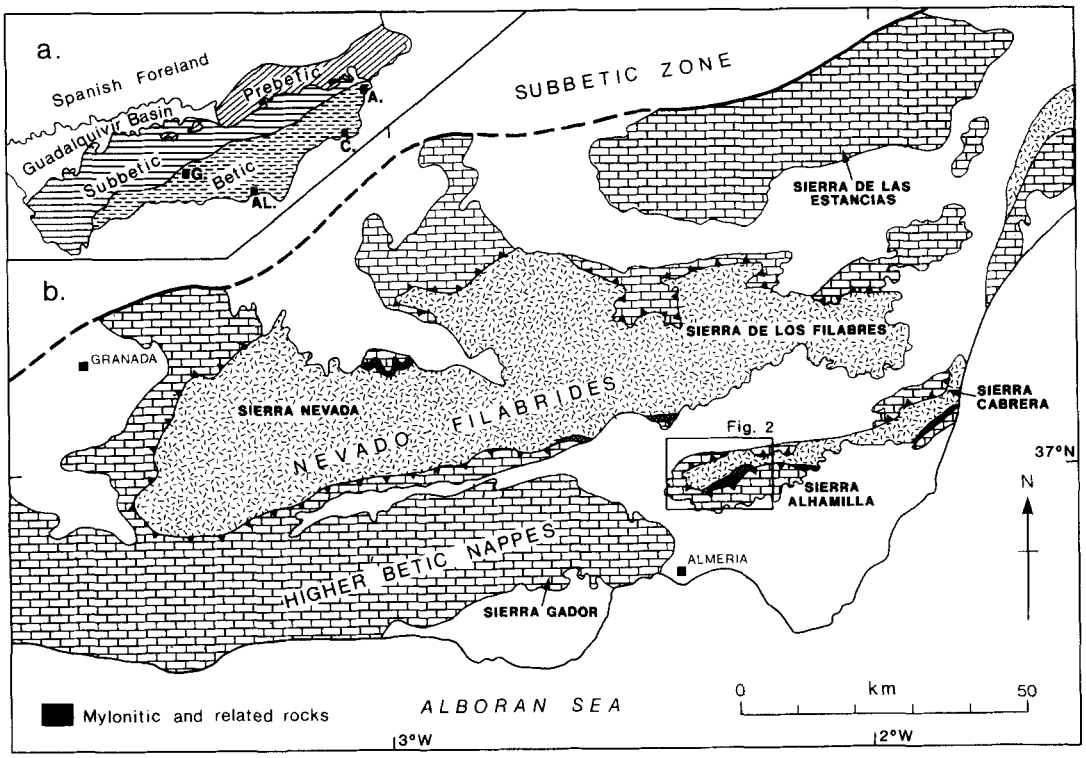

Fig. 1. (a) Tectonic subdivisions of the Betic Cordillera, S. Spain. A, Alicante; C, Cartagena; Al, Almería; G, Granada. (b) Tectonic sketch map of the eastern Betic Zone. 'Higher Betic Nappes' include Alpujarride and Malaguide complexes. Presently known exposures of mylonitic and cataclastic rocks belonging to the Betic Movement Zone shown by dense stipple.

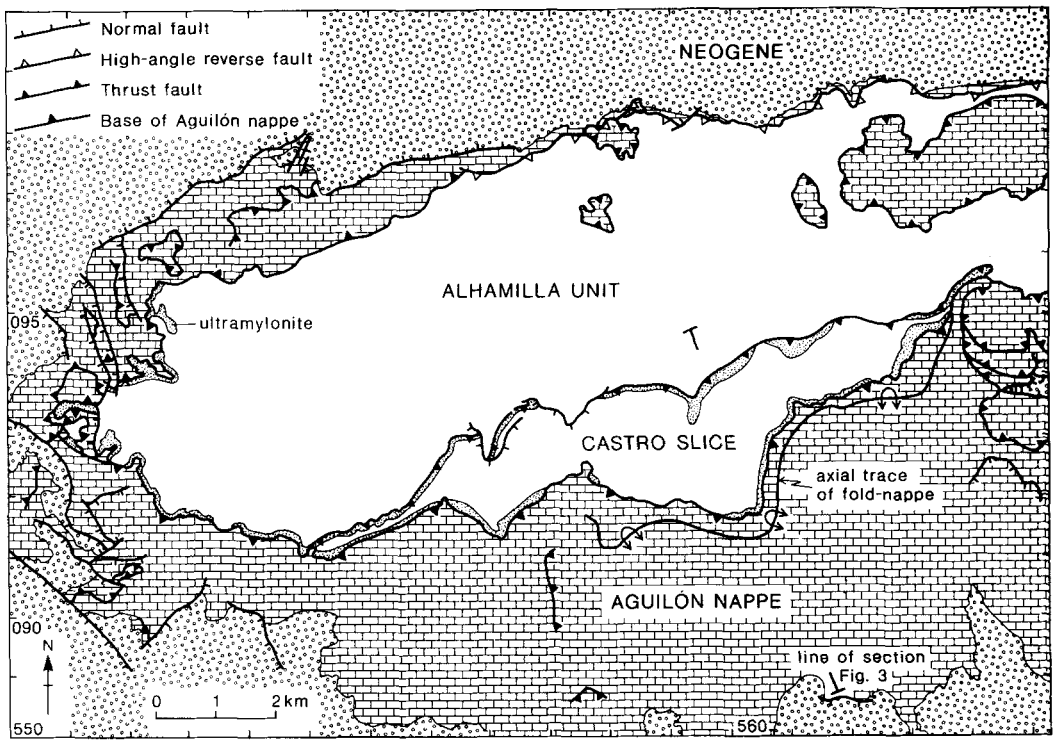

Fig. 2. Structural sketch map of the Sierra Alhamilla, modified from Platt *et al.* (1983). Brick pattern, Aguilón nappe; unornamented, Nevado–Filabride rocks; stipple, ultramylonite; open circles, Neogene.

and Platt *et al.* (1984) have shown that it is traceable over a considerable area (Fig. 1). The purpose of this paper is to document the structures and fabrics in the BMZ in its area of best development—the Sierra Alhamilla (Figs. 1 and 2).

GEOLOGICAL SETTING

The Betic Movement Zone (BMZ) in the Sierra Alhamilla is a zone of heterogeneous ductile shear up to 400 m thick beneath the Aguilón nappe, the lowest of the

Higher Betic Nappes (Figs. 2 and 3). The lower part of the Aguilón nappe itself was highly deformed during its emplacement (Platt *et al.* 1984), and in a sense therefore also belongs to the BMZ. There is an abrupt change in deformational style at the base of the nappe, however, marked by the appearance of mylonitic microstructures in the underlying rocks. This contact was a fundamental mechanical boundary during deformation, and we treat it here as the top of the BMZ. The BMZ itself involves rocks of the underlying Nevado–Filabride Complex. It includes the Castro Slice (Fig. 2), which is a lenticular rock body bounded above and below by ultramylonite bands, and the top of the underlying Alhamilla Unit. The intensity of deformation decreases gradationally downwards within the Alhamilla Unit, and no sharp lower boundary to the BMZ exists.

The Alhamilla Unit (Fig. 4) consists largely of graphitic mica–schist, grey quartzite and quartz–pebble conglomerate, metamorphosed under upper greenschist facies conditions. The Castro Slice is more heterogeneous: in addition to graphitic mica–schist and quartzite, it includes light-coloured aluminous mica–schist, marble, tourmaline-bearing quartz–feldspar gneiss, and hornblende schist, metamorphosed under lower amphibolite-facies conditions. Both units have been affected by several phases of tight to isoclinal folding, which have effectively transposed the bedding. No way-up indicators or fossils are preserved, so stratigraphic sequences cannot be established.

These units, the Aguilón nappe, and the overlying Mid- to Late Miocene post-nappe sediments, were thrown into a large faulted anticlinorium during Late Miocene tectonism, so that the BMZ is now seen in a tectonic window through the Aguilón nappe.

STRUCTURAL HISTORY

The small- to medium-scale structure of the BMZ is dominated by the effects of a phase of tight folding, intense ductile deformation, and retrogressive metamorphism, which we refer to as the main-phase deformation. This deformation followed an unknown number of earlier events, some of which occurred during the Hercynian or earlier orogenies. It would therefore be misleading to assign a number to this event, so we label it D_s. Later structures are labelled D_t, D_u, etc. in alphabetical order, and earlier ones as D_r, etc.

The main-phase structures are the earliest in a suite of progressively formed sets of structures that is restricted to the BMZ; and we suggest on these grounds that the whole suite is related to the emplacement of the Higher Betic Nappes. The suite comprises the following. (1) The main-phase structures (D_s). (2) Extensional crenulation cleavages. (3) Mylonitic foliation and syn-mylonite folds in several thin zones of very high strain: notably the Fuentes mylonite, at the base of the nappe, and the Cuillas mylonite, at the base of the Castro Slice (Fig. 3). (4) A post-main-phase set of folds (D_t). (5) Brittle faults, cataclasis and associated alteration.

One or more sets of folds with steep axial planes and variable trends postdate nappe emplacement, and may be related to the late Tertiary faulting and arching of the Sierra Alhamilla. They are shown on the sections as D_u.

PRE-MAIN-PHASE HISTORY

The main-phase deformation has largely obscured the earlier tectonic and metamorphic history of the rocks in the BMZ, so that our reconstruction of these early events is necessarily incomplete. A pre-main-phase differentiated crenulation cleavage (S_r) is well preserved in mica–schist from the deeper parts of the Alhamilla Unit, and is locally associated with isoclinal folds in bedding. It appears to have been broadly associated with the metamorphic culmination. This produced greenschist-facies assemblages in the Alhamilla Unit, including garnet, biotite and albite in mica–schist, and chloritoid in quartzite. Garnet and biotite have been widely retrogressed to chlorite, however, and no trace remains in many samples. Chloritoid locally shows rotational inclusion patterns, and albite contains helicitic inclusions showing a variable degree of development of

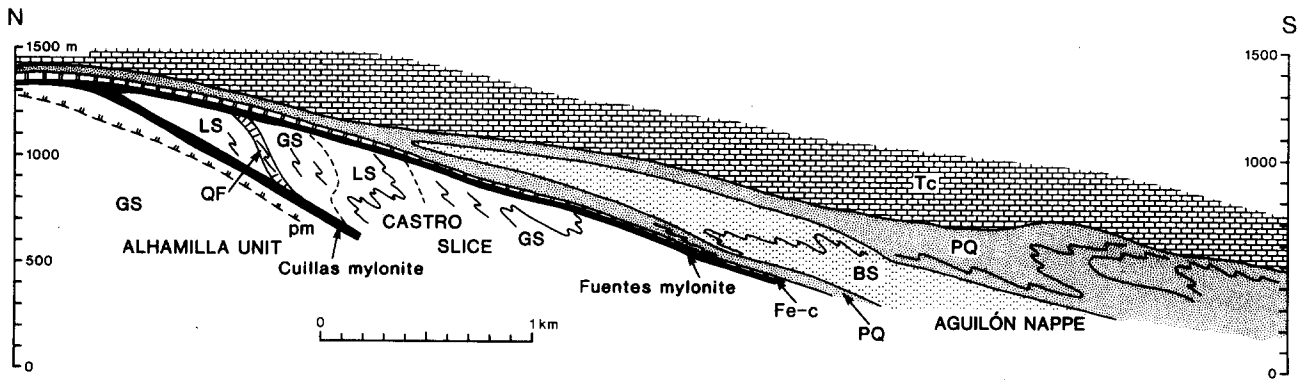

Fig. 3. Generalized structural cross-section across the southern half of the Sierra Alhamilla (for location see Fig. 2). Data have been projected in from either side onto the profile, so the topographic surface has been omitted. Aguilón nappe: Tc, Triassic carbonate rocks; PQ, phyllite and quartzite; BS, black mica schist; Fe-c, mineralized carbonate breccia and calc-mylonite. Castro Slice and Alhamilla Unit: GS, grey mica schist and quartzite; LS, light-coloured mica schist, quartzite, and marble; QF, quartz–feldspar gneiss; dense stipple, ultramylonite; pm, lower limit of mylonitic and protomylonitic microstructures.

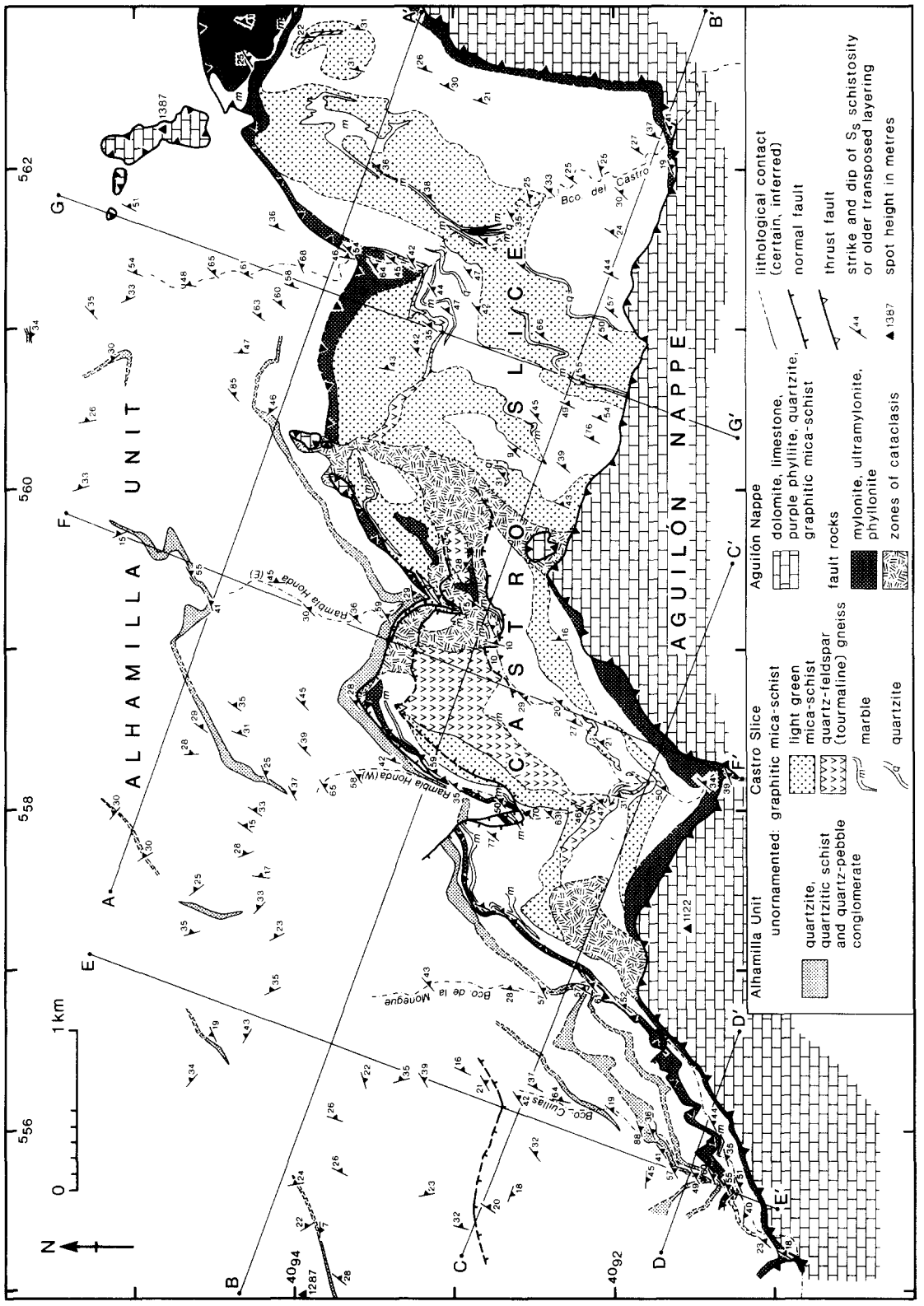

Fig. 4. Geological map of the central Sierra Alhamilla.

a crenulation cleavage, suggesting that these minerals grew during D_r. Albite always includes garnet. Our tentative conclusions based on these relationships are summarized in Table 1.

In the Castro Slice, pre-main-phase metamorphic assemblages are of the amphibolite facies, including quartz + white mica + biotite + garnet + staurolite ± kyanite ± intermediate plagioclase ± epidote in mica schist, calcite ± epidote ± green amphibole in marble, hornblende + epidote ± calcic plagioclase (up to An_{75}) ± garnet in hornblende schist, and quartz + sodic plagioclase + white mica + biotite + tourmaline ± K-feldspar in gneiss. Staurolite porphyroblasts show two stages of growth. Large crystals (up to 1 cm) contain gently curved inclusion trails, indicating growth and rotation during early stages of D_r. The grains were then corroded, followed by a later stage of growth, inter-kinematic between D_r and D_s, during which smaller grains of staurolite formed in the groundmass. The staurolite includes garnet, which predates the foliation

Table 1. Relations between deformation and metamorphism in the Alhamilla Unit

	Mineral growth	Deformation processes
D_s	Chlorite, white mica	Crystal plasticity and dynamic recrystallization of quartz in quartzite; solution transfer in mica–schist. Limited recrystallization of white mica. Retrogression.
D_r	Albite, chloritoid, biotite	Solution transfer of quartz.
	Garnet	

Table 2. Relations between deformation and metamorphism in the Castro Slice

	Mineral growth	Deformation processes
D_s	Chlorite, white mica	Crystal plasticity and dynamic recrystallization of quartz. Brittle deformation and limited recrystallization of white mica. Retrogression.
	↑	
	Plagioclase staurolite (2)	
D_r		Solution transfer of quartz.
	↑	
	Staurolite (1), kyanite, biotite? muscovite?	
D_q	Garnet	

(S_q) within the staurolite (Fig. 10a), and larger garnets commonly contain curved inclusion trails, indicating growth during D_q. Plagioclase postdates staurolite, and appears to have grown both before and during D_s. Our conclusions based on these relationships are summarized in Table 2, but we emphasize that they are based on microstructural evidence only: the regional significance of the pre-main-phase deformations cannot be assessed.

The pre-main-phase history therefore appears to have involved at least two phases of deformation accompanying a medium P/T ratio metamorphic event. This is characteristic of the second Alpine metamorphism elsewhere in the Nevado–Filabride Complex (Nijhuis 1964, Diaz de Federico *et al.* 1978, Vissers 1981), and it must have preceded the emplacement of the Higher Betic Nappes, which occurred under lower greenschist facies conditions (Platt *et al.* 1983).

Near the top of the Castro Slice in the Rambla Honda (Fig. 2), graphitic quartz–mica schist contains the pre-main-phase assemblage garnet + staurolite + chloritoid + andalusite. Main-phase deformation is intense, and the time relations of these minerals are unclear, but we suggest that the andalusite may be relict from the low P/T ratio 'pre-Alpine' metamorphic event recorded from Nevado–Filabride rocks in the Sierra Nevada by Diaz de Federico *et al.* (1978).

MAIN-PHASE STRUCTURES

Main-phase structures encompass the most prominent set of tight mesoscopic folds (Fig. 10b) and associated foliations and lineations. The folds, accompanied by substantial ductile strain, have effectively transposed both bedding and the older schistosity into a new orientation. The most prominent fabric in the rocks is usually this rotated and modified combination of bedding and pre-main-phase schistosity. Both these fabrics pass around the hinges of main-phase folds, and a new axial-plane fabric is rarely visible in the field, particularly in the Castro Slice. This can cause some difficulty in identifying main-phase structures. A pronounced penetrative stretching lineation, L_s, defined by oriented grains and grain aggregates (Fig. 10c) is widely developed, however, and provides a useful 'marker' for identifying main-phase effects in the field. Orientation data for D_s folds and L_s are shown in Figs. 5-7.

The character of the main-phase structures changes downwards away from the nappe contact. Main-phase folds are ubiquitous in the Castro Slice and in the upper part of the Alhamilla Unit, and fold hinges lie within 10° of L_s, which is strongly developed in all rock-types. Folds are less common in the deeper parts of the Alhamilla Unit (partly because of a scarcity of competent bedded units), L_s is less intense and is only visible in quartzite, and fold hinges diverge by up to 40° from L_s. Two main-phase linear fabrics can then be distinguished: the stretching lineation, and an intersection lineation between bedding and S_s. The fold-hinges therefore appear to have been rotated towards L_s and the finite elongation direction X by an amount that decreases downwards. These changes are associated with a downward decrease in strain and with a change in the dominant microstructure, as described below. Although main-phase strain is less intense at depth, S_s takes on the character of a differentiated crenulation cleavage, and is therefore more readily distinguishable as a discrete foliation than in the Castro Slice.

Changes in vergence (sense of asymmetry) of main-phase folds suggest the existence of larger scale structures (Figs. 6, 8 and 9). The present fold vergences, of course, may have little direct significance, as the fold hinges have been rotated to an unknown extent during D_s. There is also the possibility that changes in minor fold vergence may have been induced by rotation of different folds in opposite directions towards X. This process should led to the formation of sheath folds (Quinquis *et al.* 1978), and of fold hinges swinging through more than 90° across the Y direction of strain. We have not found any main-phase sheath folds, however, and the fold hinges never deviate more than about 40° from the regional trend (Fig. 6). We think that the major structures shown in Figs. 8 and 9 are real, therefore. The major folds do not always coincide with repetitions of lithological units, however. This may partly be due to the existence of older structures; but the main cause is likely to be excision of fold limbs by ductile faulting. Both the Fuentes and Cuillas mylonites locally coincide with the limbs of major folds (Figs. 8 and 9); and other thinner ultramylonite bands, not all of which are readily detectable in the field, cut the Castro Slice. The repetition of the

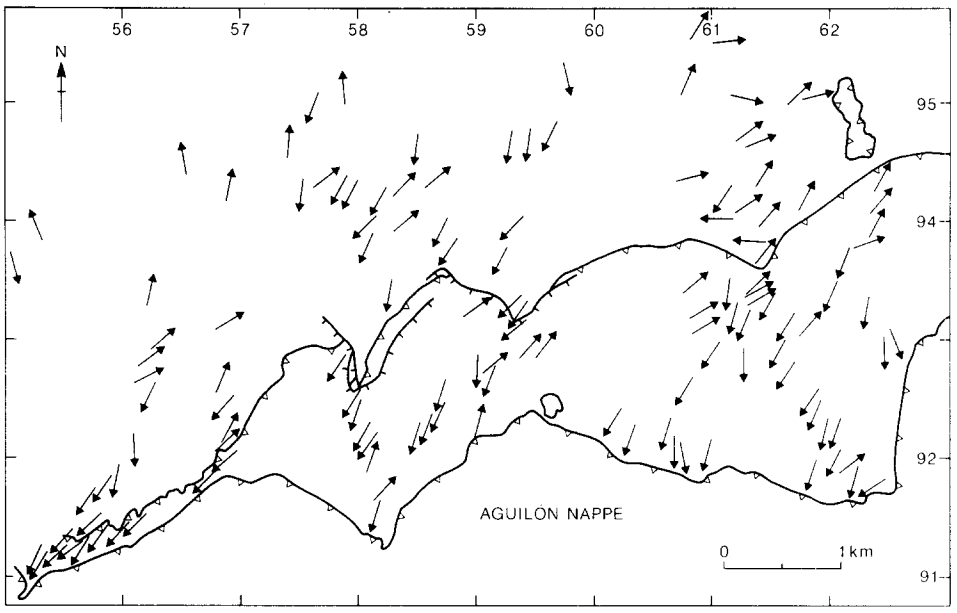

Fig. 5. Stretching lineations (L_s) in the Betic Movement Zone, central Sierra Alhamilla. Each symbol is a mean of between 3 and 20 outcrop measurements.

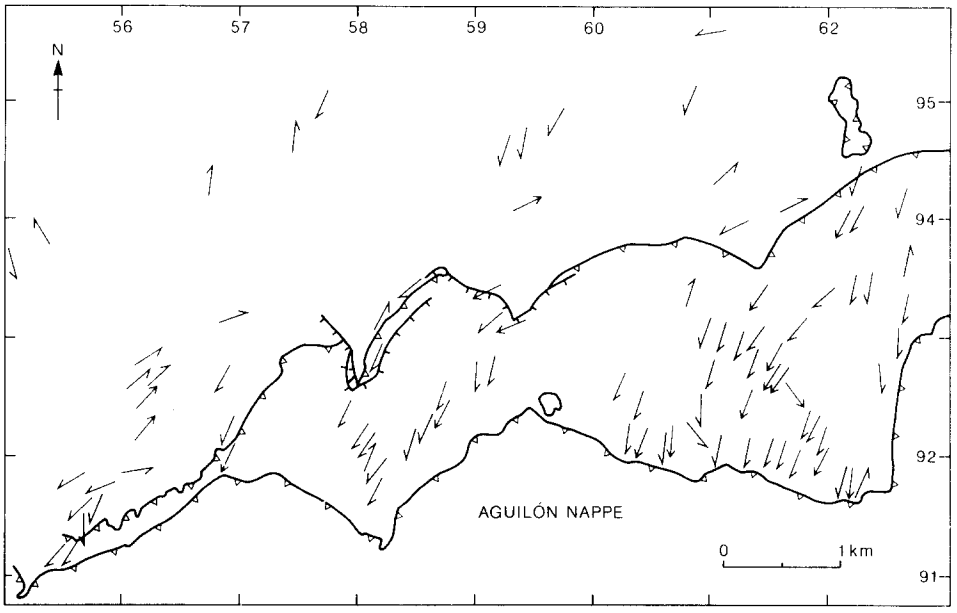

Fig. 6. Map of main-phase fold vergences in the central Sierra Alhamilla. The arrow shows the plunge direction, and the half-barb indicates the direction of vergence. An E-vergent fold has the half-barb on the east side of the arrow, for example. A double barb indicates symmetrical folds. Each symbol represents the overall vergence over 20–50 m of section. Major folds based on these data are shown in the cross-sections (Figs. 8 and 9).

conglomeratic quartzite horizon shown in the centre of section A-A′ (Fig. 8) does not coincide with a main-phase fold, and this may reflect an older structure.

Main-phase microstructure

Quartz. In some quartzites of the Castro Slice, a pre-main-phase population of annealed 50–200 μm quartz grains can be identified. These were probably roughly equant originally, but were internally deformed and partly recrystallized during the main phase into ellipsoidal lenticles that define S_s and L_s. The aspect ratio of these deformed grains allows a rough measure of D_s strain (Fig. 12). This assumes a pre-D_s equant shape, but measurements taken around a D_s fold suggest that this approximation is correct within the measurement error. Quartz ribbons produced by kinking (Figs. 11a & b) and grains affected by strong marginal recrystallization were avoided (see Behrmann 1984a for further discussion of methods and results). Figure 12 shows that strain is generally highest in the Castro Slice; that is, closest to the base of the Aguilón nappe. The microstructure of deformed quartz grains shows features characteristic of a variable degree of crystal–plastic deformation and associated dynamic recrystallization, including undulatory extinction, subgrain formation, and the development of small new grains along grain boundaries and along deformation bands within grains (Fig. 11). These microstructures are characteristic of dislocation creep processes in quartz (White 1976). The

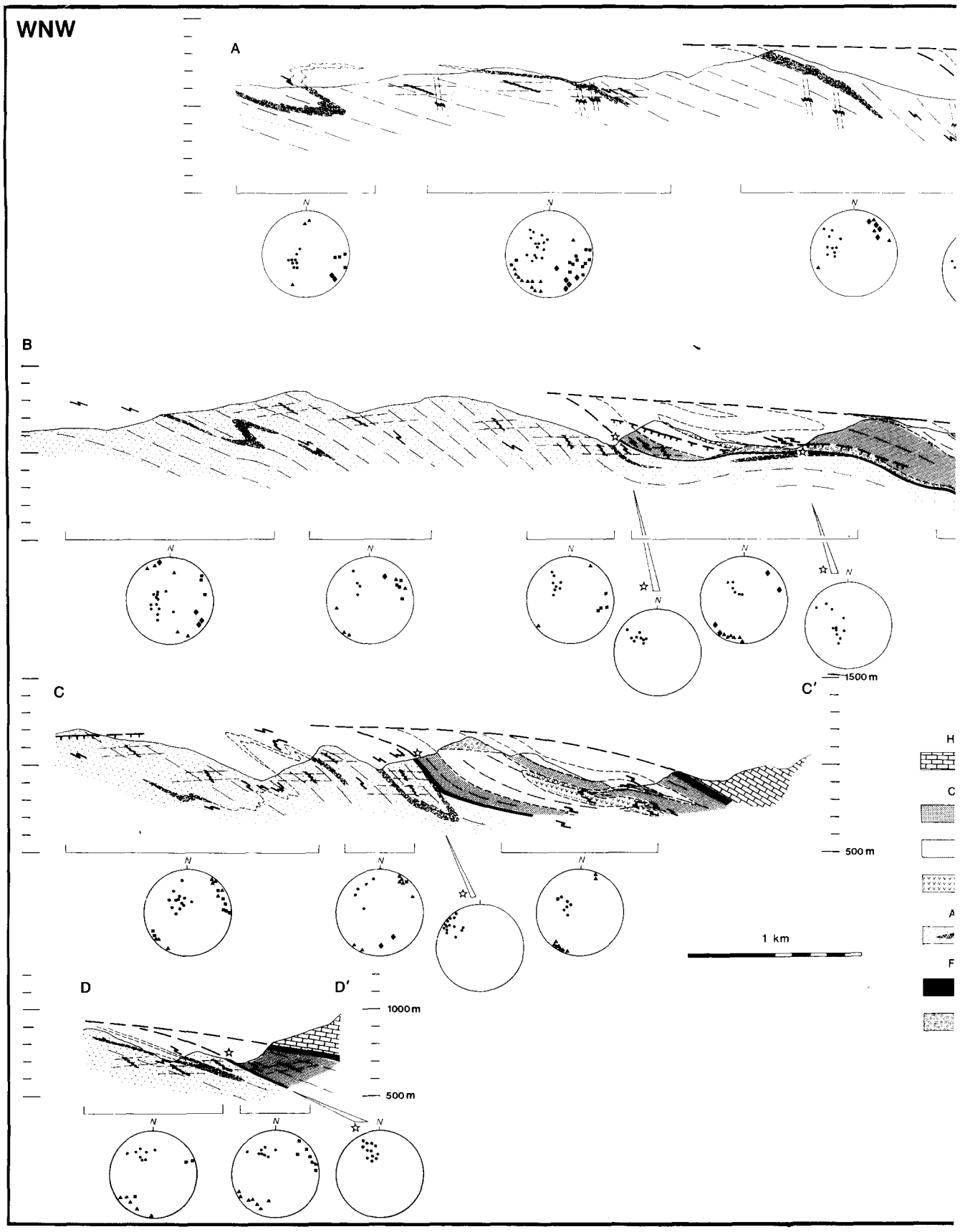

Fig. 8. Structural sections through the BMZ, normal to main-phase folds and stretching lineations. See Fig. 4 for locations. Small-scale fold vergences indicated schematically. These sections show the discordance between the overlying nappe and the structures in the BMZ, and illustrate the major folds inferred from the small-scale structures.

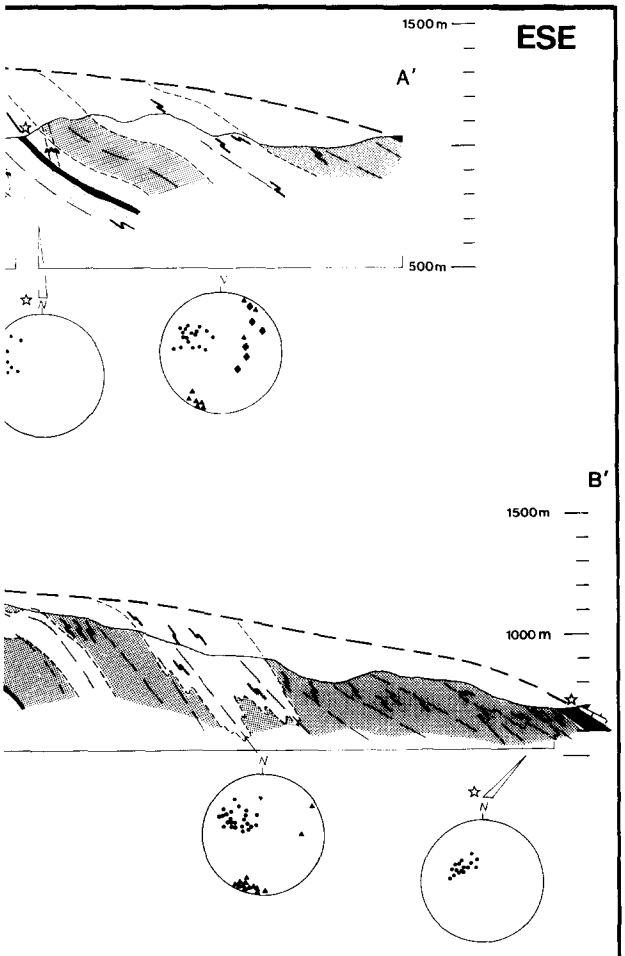

IGHER BETIC UNITS

ASTRO THRUST SLICE

grey micaschist

light green micaschist

qtz-fs-tou gneiss

LHAMILLA UNIT

silver-grey micaschist (quartzite & qtz schist)

AULT ROCKS

mylonite

zones of cataclasis

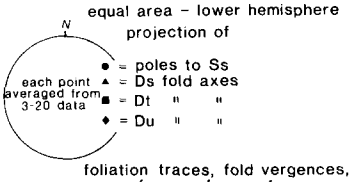

equal area – lower hemisphere projection of

● = poles to Ss
▲ = Ds fold axes
■ = Dt " "
◆ = Du " "

foliation traces, fold vergences, form surfaces of:

Ds

Dt

Du

thrust fault

normal fault

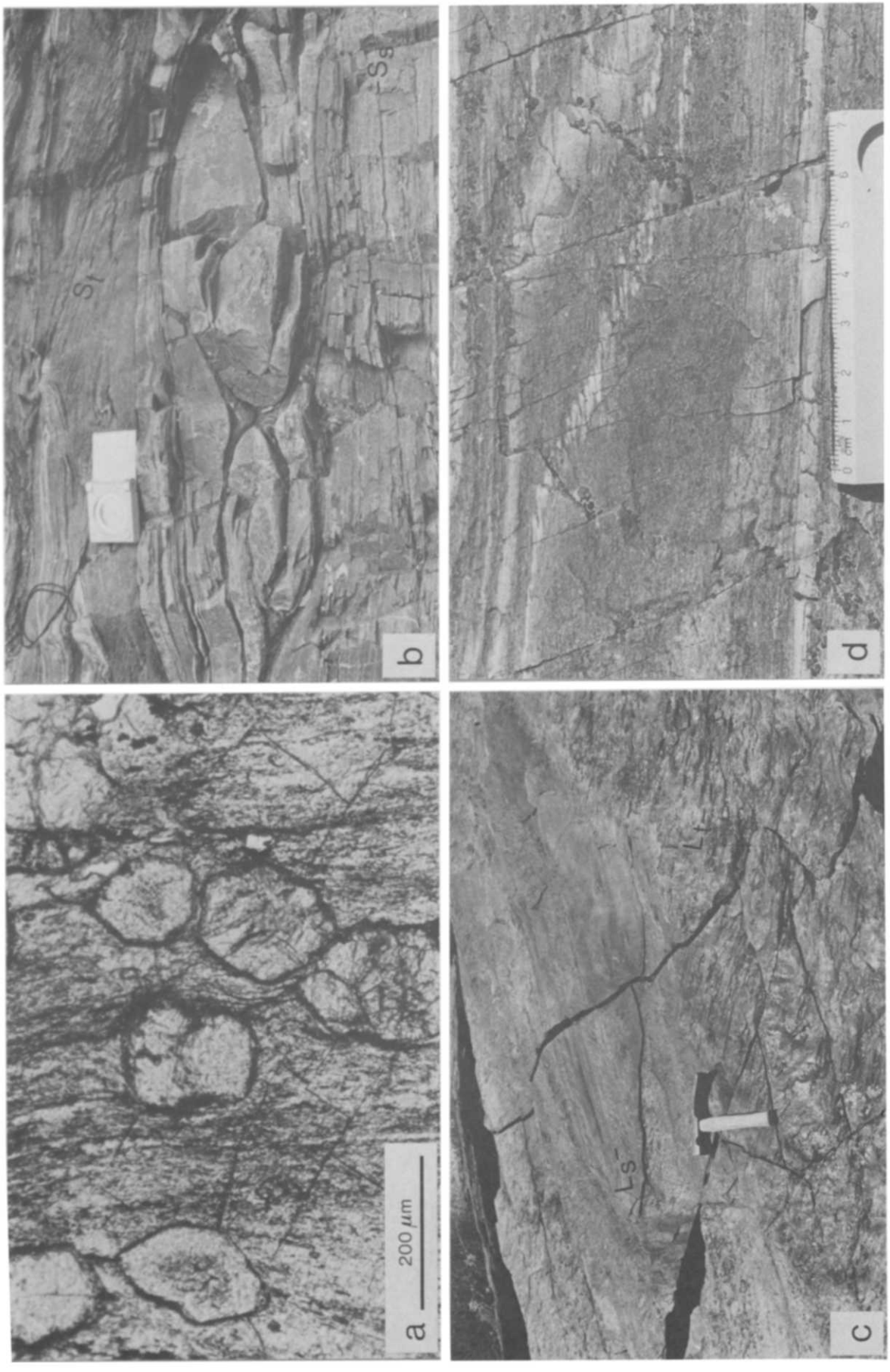

Fig. 10. (a) Small garnets included in a staurolite porphyroblast, which occupies the whole field of view (note mineral cleavage traces). Graphite defines a foliation included in the staurolite, but external to the garnet. The foliation has been flattened around the garnet and there is a suggestion of deformation shadows. Pt 459. (b) NW-vergent main-phase folds in quartzite at the top of the Alhamilla Unit, Barranco Cuillas, looking SW. Note S_s in quartz–schist at bottom, and the later crenulation cleavage (S_t) and small S-vergent D_t fold in mica–schist at top. (c) Main-phase foliation surface in mica–schist, showing the stretching lineation L_s in quartz–schist (top) and the later crenulation lineation L_t in mica–schist (bottom). The boundary between the quartz–schist and mica–schist is the intersection of bedding with S_s, which is nearly parallel to L_s. Alhamilla Unit, Barranco Cuillas. Top is NW. (d) Cuillas mylonite showing mylonitic banding and syn-mylonite folds. Barranco Cuillas, looking S. Outcrop surface is normal to the stretching lineation.

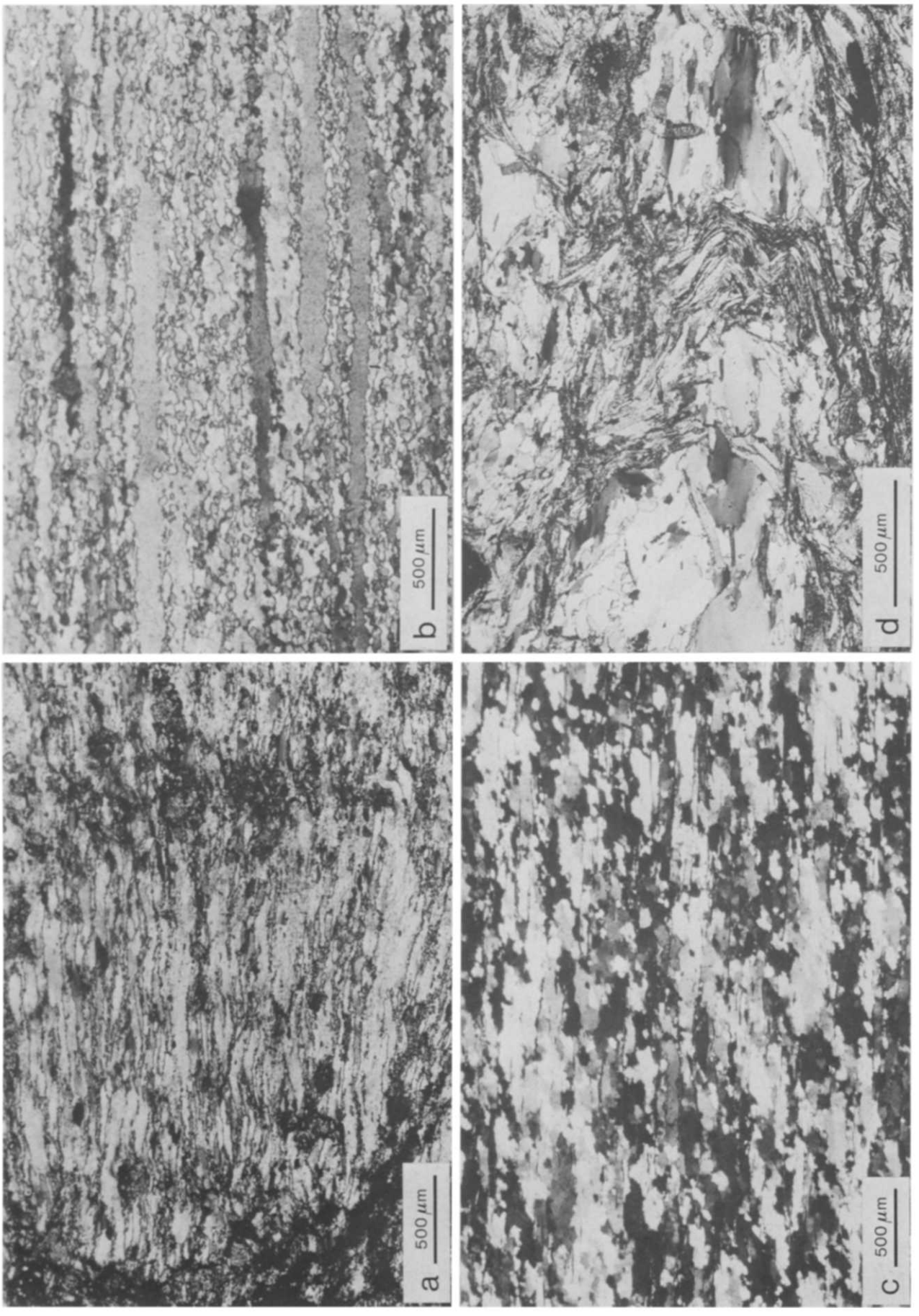
a
500 μm
b
500 μm
c
500 μm
d
500 μm

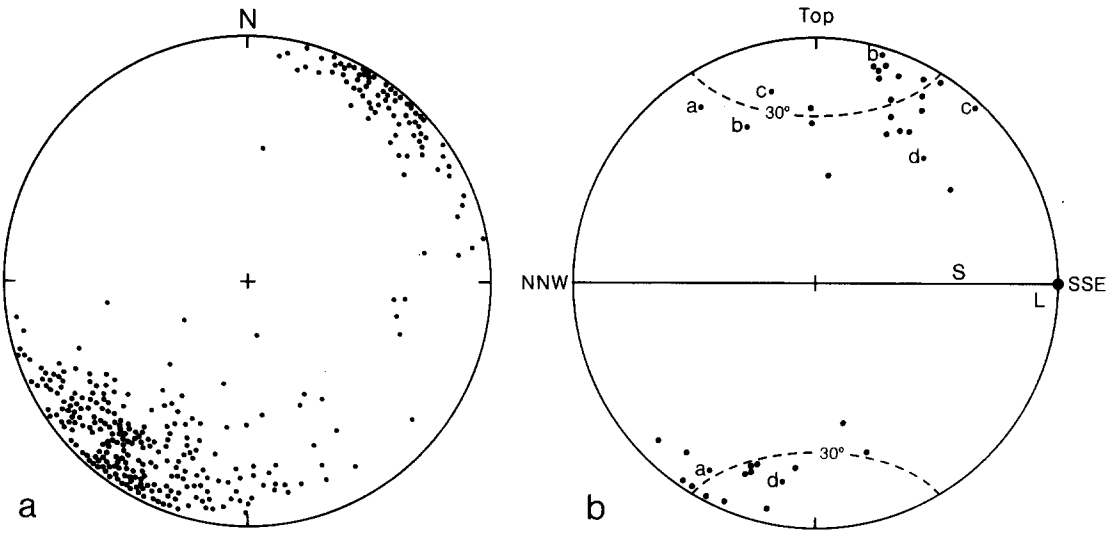

Fig. 7. (a) Main-phase elongation lineations (L_s) from the Castro and Alhamilla Units. (b) Poles to extensional crenulation cleavages, normalized to the main-phase foliation (S) and elongation lineation (L). A 30° small circle about the pole to S is shown for reference. Pairs of letters show poles to conjugate pairs of *eccs*.

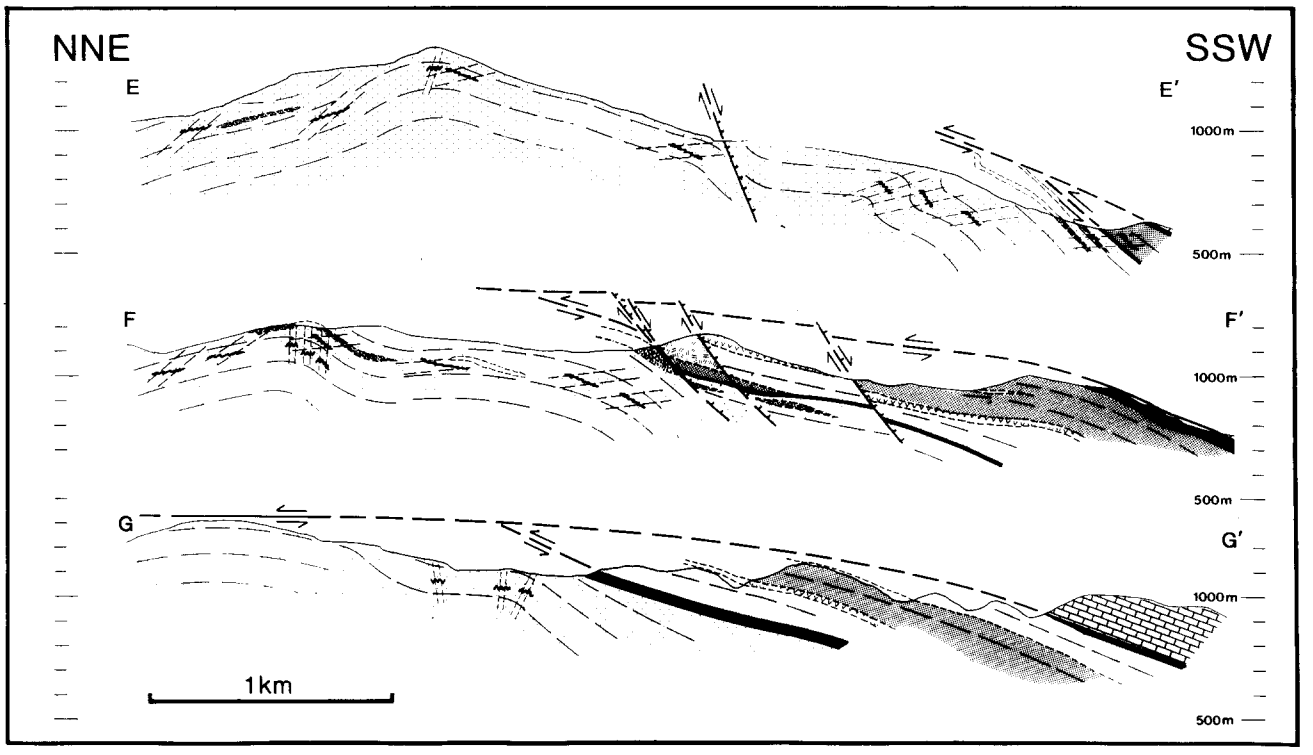

Fig. 9. Structural sections parallel to the main-phase stretching lineation, and hence to the probable direction of nappe transport. For explanation of small-scale structural symbols see legend to Fig. 8.

Fig. 11. Main-phase microstructure. (a) Main-phase fold-hinge in quartzite, cut normal to the foliation, the hinge-line, and L_s. Dark bands trending up and down at right and left are layering. Quartz ribbons define the shape fabric S_s. These are probably produced in part by kinking of pre-existing coarse-grained quartz, and hence do not directly indicate D_s strain. Note dynamically recrystallized grains: mean grain-size is 12 μm. This specimen has an unusual single girdle *c*-axis fabric with two maxima (Fig. 13). Pt 207, Castro Slice, Barranco de Castro. (b) Quartz ribbons in mylonitic quartzite, cut normal to S_s, parallel to L_s. Note roughly alternating bands of different birefringence and degree of recrystallization, produced initially by kinking. Pt 291. (c) Quartzite with extensive dynamic recrystallization cut normal to S_s, parallel to L_s. Thin horizontally oriented micas are inherited from S_r, now transposed. Crude horizontal shape fabric of quartz is S_s. New 25–50 μm grains define a shape fabric (top right to bottom left). This may lie close to the incremental elongation direction; if so, this allows determination of the sense of shear (top to right). Pt 246, Castro Slice, Colativí. (d) Crenulated mica-schist, cut normal S_s and L_s. The crenulated fabric is a 1–2 mm differentiated quartz–mica foliation (S_r), trending roughly up and down. Mica was crenulated, and quartz underwent plastic deformation during D_s. No differentiation occurred during D_s, hence S_s is defined only by kink-band boundaries in mica and the shape fabric in the quartz. Pt. 478, Castro Slice, Barranco de Castro.

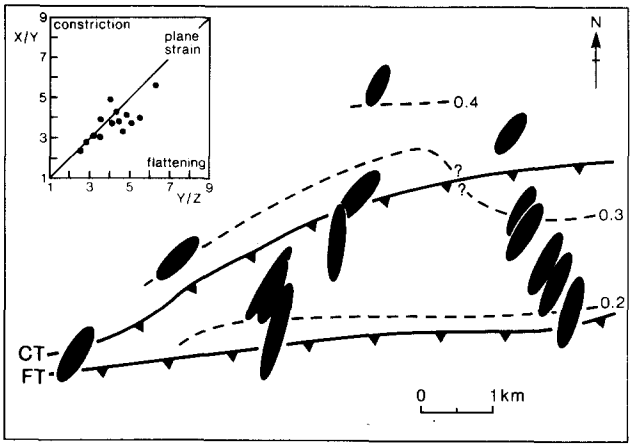

Fig. 12. Strain variation in the BMZ illustrated by *XY* sections through the main-phase finite-strain ellipsoids (ellipses), and by the magnitude of the principal stretch along *Z* (contours). The Cuillas (CT) and Fuentes (FT) thrusts are projected onto a S-dipping plane defined by the valley floors along which the specimens were taken. Inset: Flinn plot of the strain data.

size of the new grains varies (Figs. 11a & c), and this has been used by Behrmann (1984a) together with measurements of dislocation density, to help constrain estimates of flow stress and strain rates. Some of the more intensely recrystallized quartzites show, in addition to a shape fabric defined by the deformed pre-main-phase grains, a weak secondary shape fabric defined by the new grains (Fig. 11d). This phenomenon has been described by Law *et al.* (1984) and Lister & Snoke (1984), who suggest that it can be used as an indicator of the sense of shear. Lower in the BMZ, in the Alhamilla Unit, strain is generally lower, the recrystallized grain size is greater, and the degree of recrystallization is commonly higher than in the Castro Slice. These changes probably reflect lower flow stress and greater availability of water at depth (see below).

Mica. Micaceous rocks in the Castro Slice contain sheaves of white mica up to 5 mm across. These probably represent single grains formed during the metamorphic peak, but they now consist mainly of aggregates of 50–200 μm sub-parallel grains. The latter are locally bent, pinched, and crosscut by discrete brittle fractures. Behrmann (1984b) reports transmission and scanning electron microscope observations of cracking along the basal planes, suggesting that mica deformation was achieved by a combination of flexure and brittle deformation. New grains up to 50 μm long have grown locally at the expense of the deformed aggregate. This phase of grainsize reduction and recrystallization appears to have been isochemical (Behrmann 1984b).

In the hinges of main-phase folds, mica defining the older foliation is tightly crenulated on a scale between 0.5 and 10 mm (Fig. 11d). These compressional crenulations are irregular and disharmonic, and sometimes form conjugate sets of kinks. No differentiation has occurred, so that mica-rich cleavage zones have not formed. This accounts for the lack of a good mesoscopically visible axial-plane S_s.

In main-phase fold limbs, the mica sheaves and laminae are commonly crosscut by discrete microshear zones, which form sets with a roughly regular spacing and orientation. These define single or conjugate sets of extensional crenulation cleavages (Platt & Vissers 1980). The significance of these cleavages is discussed in more detail below. Towards the margins of the cleavage zones, the mica has been reduced in grainsize to about 5 μm. Microchemical studies (Behrmann 1984b) demonstrate that this new mica is significantly richer in iron than the old mica, and was formed in a second phase of non-isochemical recrystallization. These two phases of recrystallization probably occurred during a single progressive deformational event, during which the temperature decreased, the fluid composition changed, and the bulk rock rheology was modified by the increasing strength of the foliation and the decreasing grainsize.

Grey mica–schists in the Alhamilla Unit, below the Castro Slice, show a distinctly different main-phase microstructure, and the change occurs fairly rapidly below the Cuillas mylonite. Compressional crenulations of the older foliation are more widespread, and are most common in main-phase fold hinges. These crenulations are more regular than in the Castro Slice, and are differentiated to produce a characteristic banded foliation. Where main-phase crenulations are not developed, the main effect of D_s seems to have been to intensify the pre-existing foliation (S_r). The intensity of extensional crenulation cleavages is considerably less, and their spacing greater, locally up to several metres. These changes generally reflect the increased importance of pressure–solution processes in deformation vs crystal–plastic processes. This change in the dominant deformation mechanism is likely to have been in part a result of the lower D_s strain (Fig. 12) and flow stress (Behrmann 1984a) below the BMZ; but an additional factor may have been the availability of water. Widespread main-phase retrogression (i.e. hydration) of amphibolite-facies minerals is likely to have considerably reduced water activity in the Castro Slice, whereas water-consuming reactions were substantially less important in the originally lower-grade Alhamilla Unit.

Extensional crenulation cleavages

As mentioned above, micaceous rocks in the BMZ are commonly cut by one or more sets of extensional crenulation cleavages (*ecc*). These cleavages are oblique to S_s, but we relate them to D_s on the following grounds. (i) Where quartz-rich and mica-rich rocks are interlayered, the quartz-rich rocks lack *eccs* and show a homogeneous main-phase microstructure as described above. The interlayered micaceous rocks, however, show one or more sets of these cleavages, and quartz grains dispersed in the mica are significantly less deformed than those in the quartzose layers. Much of the D_s strain in the micaceous rocks has therefore been taken up by shear on the cleavage-zones. (ii) The effects of the cleavages is always to cause extension in the plane of S_s. (iii) There is a spatial correlation between the magnitude of D_s strain (Fig. 12) and the development of *eccs*. They are most abundant and most closely spaced (1–2 mm) in the

micaceous mylonites and in the Castro Zone; and they disappear downwards in the Alhamilla Unit, the spacing increasing to over 1 m. (iv) The cleavages are overprinted by the next distinguishable set (D_t) of folds.

The *eccs* vary considerably in their geometrical relation to S_s (Fig. 7b), although they always lie at a low angle (less than 35°) to it. They are most commonly oriented with a steeper southerly dip than S_s, so that the sense of shear on the cleavage zones is southerly: the opposite to that indicated by the quartz fabrics (see below), or by the geometry of the Aguilón nappe. Some, however, have a northerly sense of shear, but these occur mainly as members of conjugate pairs. The cleavages commonly intersect S_s at a high angle to L_s, but they are rarely orthogonal to L_s. We envisage them as having formed after D_s folds had been initiated and tightened somewhat, during the period of distributed deformation that also rotated the fold hinges and produced L_s and the dominant microstructure. The occurrence of conjugate sets, and single sets with alternating senses of displacement, suggest that flow may have deviated significantly from simple shear, and may in places have been coaxial (Platt 1984). This conclusion is also supported by our observations on the quartz fabrics (see below). Conjugate sets of *eccs* have recently been described from the mylonites along the Moine thrust by Law *et al.* (1984), who also interpret them as indicating local coaxial flow.

THE MYLONITE ZONES

Two major zones of mylonite can be mapped through the Sierra Alhamilla (Figs. 2–4). The upper, Fuentes mylonite, follows the base of the Aguilón nappe; the lower, Cuillas mylonite, marks the base of the Castro Slice.

The Fuentes mylonite varies considerably in character along its outcrop, depending on the character of the underlying rocks. It reaches its maximum development near the Cortijo del Marchal de Fuentes (582912 on the Almeria 1:50,000 topographic sheet, no. 23.43) in the Rambla Honda. Here we distinguish the following divisions, from top to bottom. (a) 6 m of foliated rauhwacke or cargneule. This consists of a very fine-grained calcite–dolomite mylonite with floating blocks of coarse-grained dolomite and calcite marble up to several cm in diameter. Fragments of mylonitic schist derived from the Castro Slice are also present locally. We interpret this carbonate zone as being derived from limestone and dolomite in the overlying nappe, as dolomite is entirely lacking in the Alhamilla and Castro Units. (b) Up to 10 m of greenish-grey banded quartz-rich ultramylonite with abundant small-scale folds. (c) Up to 40 m of blue or greenish-grey phyllonite, consisting largely of very fine-grained quartz, white mica, chlorite and albite. (d) Mylonitic schists of the Castro Slice.

Further east in the Barranco de Castro (623916), the carbonate mylonite is only ½ m thick, and lies on 5 m of pale-green flinty banded quartz-rich ultramylonite, which in turn lies on 5 m of black phyllonite. This grades down into graphitic mica schist of the Castro Slice.

To the west, in the Barranco Infierno (553914), about 10 m of iron-rich dolomitic marble forms the base of the Aguilón nappe. This lies on a heterogeneous zone of mylonitic rock including calcite marble and quartzofeldspathic gneiss of the Castro Slice. The marble has deformed very irregularly, and contains floating blocks of mylonitic schist.

The Cuillas mylonite separates the Castro Slice from the underlying Alhamilla Unit, and contains material derived from both units. Most of it is derived from the Castro Slice, however, and on the map (Fig. 4) we include it in the Castro Slice. The zone is up to 50 m thick, but both the upper and lower boundaries are diffuse, involving a gradational decrease in the intensity of the mylonitic foliation and lineation, so that they grade into the main-phase fabrics in the surrounding rocks. The zone as a whole is distinctively banded, due to the involvement of a variety of rock-types from either side, including graphitic mica–schist, green chloritic mica–schist, quartzite and quartzofeldspathic gneiss.

Microstructure of the mylonites

The Fuentes mylonite is fairly uniformly ultramylonitic, whereas the Cuillas zone contains anastomosing bands of ultramylonite a few tens of cm thick, surrounded by mylonitic schist with microstructures transitional into those of the surrounding Castro and Alhamilla schists. Both zones are characterized by a mm-scale banding defined by variations in the proportions of quartz, feldspar, white mica and chlorite. The bulk of the matrix quartz and sheet-silicates have grainsizes in the 5–10 μm range. In the more micaceous varieties the sheet-silicates are very well oriented, and the foliation is cut by single, multiple, or conjugate sets of mm-scale extensional crenulation cleavages. Porphyroclasts include feldspar and tourmaline (which show effects of brittle deformation only), mica fish, and lenticular or ribbon-shaped quartz grains. The latter show varying degrees of dynamic recrystallization and may merge into the groundmass quartz. The Cuillas mylonite also contains porphyroclasts of partly retrogressed garnet and staurolite.

The matrix quartz in the mylonites varies in grainsize from 5–10 μm in the east of the area to about 20 μm in the west (Behrmann 1982, fig. 3.6), a change which probably reflects a small gradient in temperature or water content during deformation. The grains are moderately elongate with X/Z aspect ratios of less than 1.4. Small amounts of calcite or flakes of white mica are commonly distributed along the grain-boundaries. TEM observations by Behrmann (1982) revealed the presence of subcell structures about 1 μm across within the grains, and of elliptical voids along grain boundaries. Dislocation densities in the quartz mylonites are significantly lower than those in adjacent Castro Slice quartzites. Behrmann (1982, 1985) interpreted these features, together with the *c*-axis fabric data (see below),

as indicating a switch to grain-boundary sliding as the dominant deformational mechanism in the mylonites, accompanied by a significant drop in flow-stress.

Progressive refolding in the mylonites

Locally the mylonitic foliation is deformed by families of small-scale asymmetric tight to isoclinal similar folds with axial planes at low angles to the foliation. These folds are restricted to the mylonite zones and do not affect the boundaries of the zones. Their vergence and axial orientation are variable, though many have axes close to the stretching lineation. The mylonitic banding, and ribbon quartz grains in the foliation, are clearly folded around these structures, but matrix quartz grains are commonly elongate parallel to their axial planes. These folds therefore probably nucleated after a strong foliation had already formed, as a result of flow instabilities in a highly anisotropic material (Platt 1983), and were progressively amplified, flattened and rotated during continuing flow in the mylonite zones (Carreras *et al.* 1977, Bell 1978, Quinquis *et al.* 1978).

POST-MAIN-PHASE EVENTS

A fairly consistent set of S- to SE-vergent small-scale folds with subhorizontal axial planes deform S_s in the schists, and they also deform the mylonitic foliation and the boundaries of the mylonite zones. In analytical terms these structures represent a distinct deformational event (D_t). No equivalent set of structures can be identified in the overlying Aguilón nappe: post-main-phase folds in the nappe are N-vergent with steep axial planes. Hence these structures may have formed during the later stages of nappe movement, while the base of the nappe was still a mechanical discontinuity. We cannot offer a simple or unique explanation of the S to SE vergence of the D_t folds. Possibilities include (i) a late-stage reversal of the sense of shear, analogous to the zones of 'backthrusting' in the Alps (Platt & Lister 1985); (ii) rotation and steepening of the Castro Slice, accompanied or followed by vertical shortening, as a result of movement over irregularities in the bounding fault zones (e.g. Law *et al.* 1984, fig. 18d); or (iii) heterogeneous strain caused by variable resistance to motion in the progressively hardening mylonite zones.

Zones of locally intensely brecciated and altered (albitized and kaolinized) schist and mylonite occur near the base of the Aguilón nappe, and to a lesser extent along the base of the Castro Slice. Some discrete fault-zones contain a blue–grey albite-rich rock with a microstructure suggesting repeated phases of brecciation, pressure solution, plastic deformation and albitization. These phenomena indicate a phase of dominantly brittle deformation, alternating with ductile processes (Sibson 1980). The repeated albitization may have been caused by seismic pumping induced by stick-slip motion on the faults (Sibson *et al.* 1975) during the late stages of nappe translation.

QUARTZITE FABRICS

All quartzites from the Alhamilla Unit and the Castro Slice show well developed preferred-orientation patterns of the crystallographic *c*-axes (Fig. 13). Fabrics were measured optically on a Universal Stage: between 100 and 429 grains per specimen were sampled on a squared grid, care being taken to exclude preferential sampling of grains with particular orientations or microstructures. Fabrics were plotted on lower-hemisphere equal-area projections, and contoured using a Lambert net of 206 overlapping equal-area counting circles. The patterns can be related to the main-phase finite-strain reference frame using the deformed pre-main-phase quartz grains as discussed in the section on microstructure. In the fabric diagrams, the maximum extension direction X is oriented E–W, Y is in the centre and Z N–S.

Fabric types and slip-systems

The standard pattern is a type I crossed girdle (Lister & Williams 1979) with a sharply defined outline and a tendency to develop discrete maxima of variable intensity around Y, on the central girdle segment at a 30–40° angle to Y, and next to the XZ great circle at angles between 20 and 40° to Z. Examples of such a 'complete' fabric outline are B2, B5, B102, Pt463 and Pt490 (Fig. 13). Most other specimens have a general crossed girdle pattern, but show modifications like one or two missing fabric 'legs' (e.g. B39, C5). This was explained by Behrmann & Platt (1982) as a result of uneven *c*-axis distributions prior to main-phase deformation. Only Pt207 has a distinct 'single girdle' topology oriented nearly orthogonal to the S_s trace with two maxima at angles of 30–40° to Y. Pt233 has a discontinuous, weakly defined single girdle pattern orthogonal to the S_s trace.

The intensity of the crystallographic preferred orientation is lower in the specimens taken from the very fine grained Fuentes and Cuillas mylonites (B45, Pt460, Pt488) (see Fig. 13), and the crossed girdle topology is no longer obvious in Pt460 and Pt488. This may reflect a switch in the principal deformation mechanism away from crystal plasticity. This switch appears only to have occurred in the two mylonite carpets where the dynamically recrystallized grain-size is less than 10 μm. Taken

Fig. 13. Map of *c*-axis fabrics in quartzite tectonites and mylonites, indicating specimen locations and the position of the mylonites. Lower hemisphere, equal-area projections. Contours are generally 1, 2, 3, 4, 6, 10× uniform distribution. Additionally, 5× uniform distribution is contoured in Pt 200, Pt 233, Pt 463, Pt 490, B 68 and B 102. 8× uniform distribution is contoured in B 69; 6× u.d. is left out in B 68. Number of measurements indicated on right side of each figure. The inset in the lower right hand corner explains the relationship of the crystallographic fabric to the structural elements, the D_s finite strain reference frame (X, Y, Z), and geographical directions (N to NE).

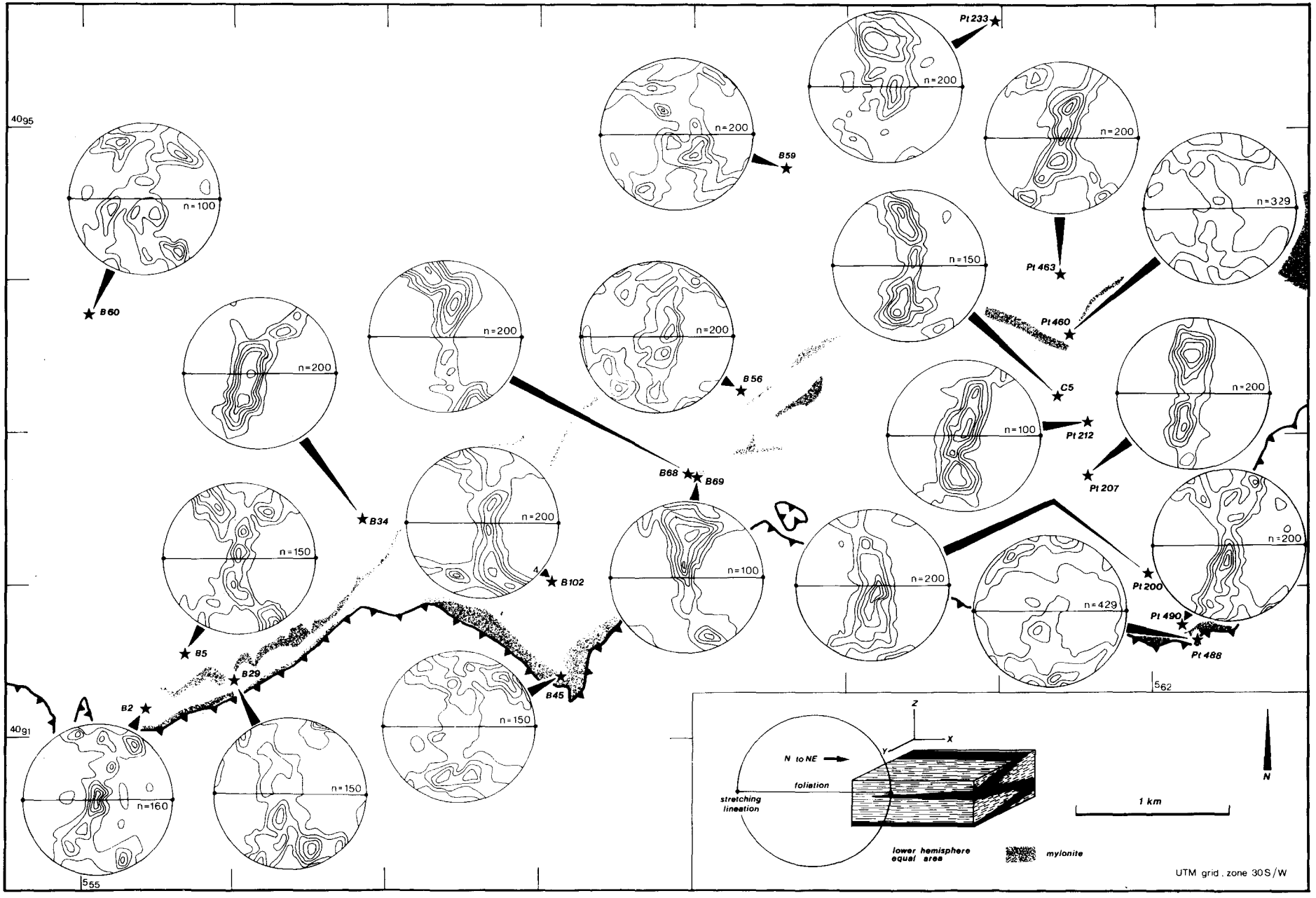
40 95
40 91
5 55
5 62
n=100
n=200
n=150
n=160
n=329
n=429
B60
B59
B56
B34
B68
B69
B102
B5
B29
B2
B45
Pt 233
Pt 463
Pt 460
C5
Pt 212
Pt 207
Pt 200
Pt 490
Pt 488
A
B
N to NE
foliation
stretching lineation
Z
X
Y
lower hemisphere equal area
mylonite
1 km
N
UTM grid, zone 30S/W

together with the TEM data discussed above, this may indicate that a grainsize-sensitive mechanism such as grain-boundary sliding became important in the mylonites.

The opening angle of a cross girdle fabric (see Lister & Dornsiepen 1982, quoting Behr 1968) is defined as the angle between the two fabric legs on the XZ great circle about Z. In our specimens this angle varies between 45° (B68) and 88° (B59). Behr (1968) was able to show that the opening angles of crossed girdles increase with metamorphic grade. The variations in our samples cannot be explained in this way, as D_s deformation appears to be accompanied by lowermost greenschist-facies conditions throughout the area. Large (>65°) opening angles however, seem to be confined to the Alhamilla unit tectonites. A comparison between opening angles and finite D_s strain (see Behrmann 1982, fig. 3.32) fails to indicate a clear interrelation, implying that the opening angle is more or less invariant with strain, and also with strain-rate, as D_s probably covered a similar time span throughout the area (Behrmann 1984a). Lister & Dornsiepen (1982) attributed the increase of opening angles with increasing metamorphic grade to a switch from $\{0001\}\langle a\rangle$ to $\{10\bar{1}0\}\langle c\rangle$ slip. One additional factor to promote this transition may be the content of kinetically active hydroxyl in the quartz (Paterson & Kekulawala 1979). Some observations of Blacic (1975) suggest that the activation of $\{10\bar{1}0\}\langle c\rangle$ slip is comparatively easy when the content of grown-in water in the crystals is high. If the hypotheses of Lister & Dornsiepen and Blacic are correct, the change in opening angle may indicate that the Alhamilla Unit quartzites were 'wetter' than the Castro Slice ones. This would be consistent with the microstructural evidence (see above). Lower water activity in the Castro Slice could have helped to reduce the kinetically active hydroxyl content in the quartz and hence inhibit the activation of prism $\{10\bar{1}0\}\langle c\rangle$ slip.

Fabric asymmetry and kinematic interpretation

Lister & Williams (1979) suggested that the asymmetry of c-axis fabric topologies (skeletons) could be used to determine the sense of shear in zones of non-coaxial flow; and this method has been applied by Behrmann & Platt (1982), Law *et al.* (1984) and others. Behrmann & Platt (1982) used twelve of the quartzites shown in Fig. 13 to determine a NNE sense of shear for the Aguilón nappe. They noted that only eight fabrics had distinctly asymmetric topologies with respect to the finite-strain reference frame defined by the axial-plane foliation (S_s) and stretching lineation (L_s), and speculated that the other, less distinctive fabrics may have been produced by deformation histories that deviated from simple shear. The fabric skeleton (Lister & Williams 1979) is derived from the contoured fabric diagram by linking up intensity peaks and crest lines by a series of straight-line segments (Fig. 14). The degree of external asymmetry of the fabric is characterized by the obliquity of the central girdle segment with respect to the foliation trace (defined by ψ in Fig. 14a). The degree of internal asymmetry is defined by the unequal inclination of the peripheral fabric legs with respect to the central girdle segment (ω_1, ω_2 in Fig. 14a). The way in which the various components of such a fabric may relate to the microstructure has recently been discussed by Law *et al.* (1984). An inspection of Fig. 13 shows that there are significant regional variations in the degree of external asymmetry (expressed by ψ). The determination of ψ involves an error (probably about ±2°) because the central girdle segments are not perfectly straight, but there appears to be a consistent pattern of variation (Fig. 15). This is best defined by the N–S sections in the east and centre of the area, and shows an increase of ψ away from the Fuentes and Cuillas mylonites towards the central portions of the Castro Slice and the Alhamilla Unit. Note that we have not included the ultramylonite bands themselves in this analysis, because the fabrics are too diffuse.

The variation of ψ is controlled by two factors. (1) The most important factor from our point of view is the degree of non-coaxiality, or vorticity (Means *et al.* 1980), of the flow. Lister & Hobbs (1980) found in their Taylor–Bishop–Hill simulations of crystal–plastic flow in quartzite that during progressive plane deformation the

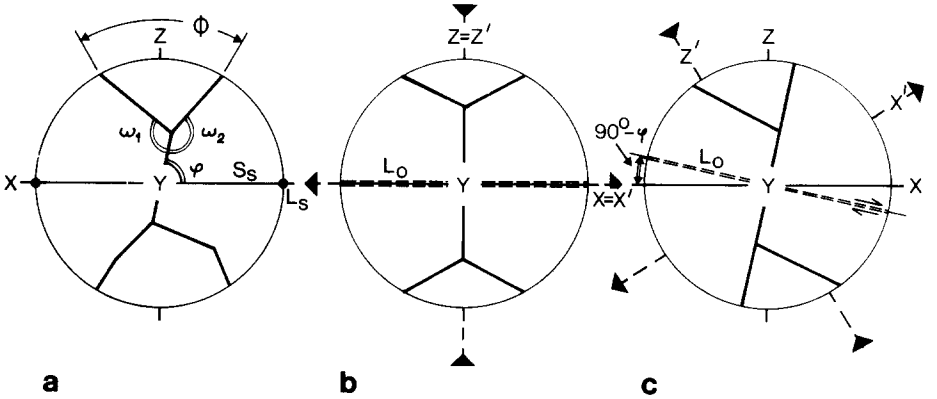

Fig. 14. Quartz c-axis fabric skeletons and their kinematic interpretation. (a) Skeleton of Pt 463. ϕ designates the opening angle, ω_1 and ω_2 characterize the internal symmetry, and ψ the external symmetry. X, Y, Z are the principal axes of finite strain, S_s is the axial plane foliation to D_s folds and L_s is the associated stretching lineation (after Behrmann & Platt 1982). (b) Fabric skeleton of model quartzite B of Lister & Hobbs (1980), coaxial deformation history, 80% overall shortening, parallel to Z, plane strain. X', Z' are the principal axes of instantaneous stretching and shortening, L_0 is a particle line of no angular velocity. (c) Fabric skeleton of model quartzite B of Lister & Hobbs (1980), progressive simple shear (γ = 4.0). W is the sense of vorticity. For further discussion see text.

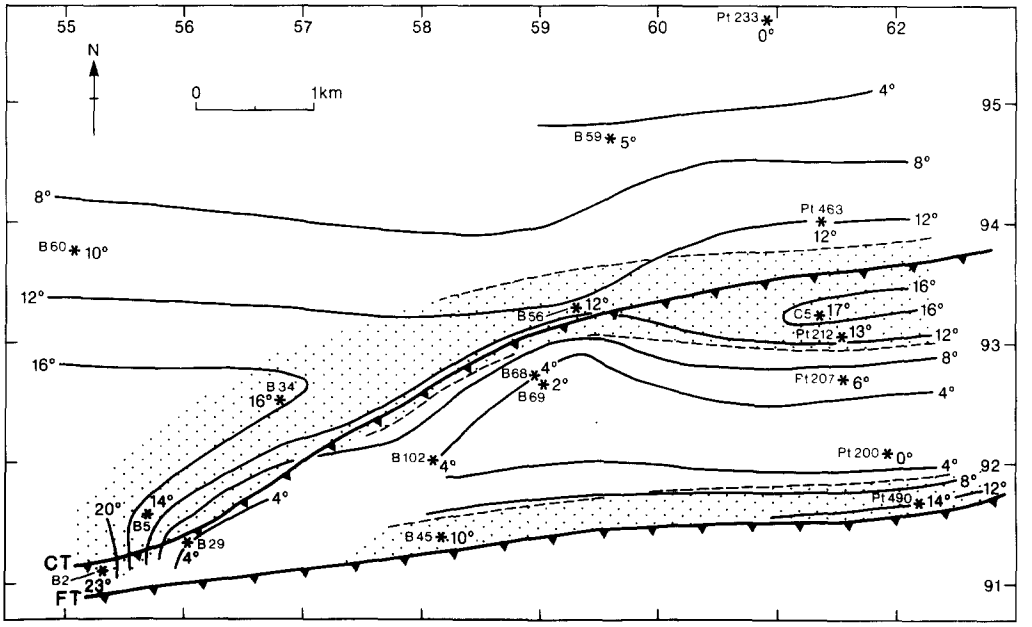

Fig. 15. Regional distribution of the degree of external asymmetry of the quartz *c*-axis fabrics. The figures given for the lines of equal asymmetry are $90° - \psi$. FT, Fuentes thrust; CT, Cuillas thrust. Contours and structural features are projected on to a S-dipping plane defined by the floors of the valleys along which the specimens were taken. Stippled areas outline regions where flow corresponds approximately to progressive simple shear, as inferred from Fig. 16 (see text for discussion).

central girdle segment established itself orthogonal to the shear plane in simple shear, and orthogonal to the XY plane of finite deformation in pure shear (see Figs. 14b & c). Note that the shear plane in simple shear is a plane of zero angular velocity, and the X and Y directions in pure shear are lines of zero angular velocity, with respect to the instantaneous strain axes. The consequences of this are that $\psi = 90°$ for pure shear, and $\psi \neq 90°$ for simple shear. (2) The use of ψ as an indicator of non-coaxial flow is complicated by the second factor: finite strain. In simple shear the XY plane of finite strain rotates towards the shear plane as strain increases, so that ψ approaches 90°.

From the above it follows that $90° - \psi$ marks the angle between the X direction and a line of zero angular velocity (the shear direction in the case of simple shear). In progressive simple shear this angle varies with respect to the maximum principal stretch according to equations 3-67 and 3-70 of Ramsay (1967)

$$(1 + e_x)^2 = \frac{\gamma^2 + 2 + \gamma\sqrt{(\gamma^2 + 4)}}{2};$$

and

$$\tan (90° - \psi) = \frac{\gamma}{1 + \gamma^2 - \dfrac{1}{(1 + e_x)^2}};$$

where $(1 + e_x)$ is the maximum principal stretch, and γ is the simple shear strain. In pure shear $90° - \psi$ remains zero, as outlined above. A graphical solution of $90° - \psi$ as a function of $(1 + e_x)$ for simple shear is given in Fig. 16, and values for $(1 + e_x)$ and $90° - \psi$ in the quartzite specimens (from Table 1 of Behrmann 1984a) are plotted on the figure. If the fabrics were produced by simple shear, they should plot along the curve. Allowing for an uncertainty of $\pm 2°$ for $90° - \phi$ and $\pm 13\%$ for X (see discussion in Behrmann 1982, p. 84), we can see that several specimens plot well below the curve for simple shear. We interpret this as reflecting an effective deviation from progressive simple shear at hand-specimen scale in these samples. Their deformation history is probably best described as intermediate between simple shear and pure shear, with the exception of Pt200, which lies neatly on the horizontal axis, indicating pure shear.

Going back to the regional distribution, we observe that fabrics approximating simple shear (stippled area in Fig. 15) are concentrated next to the Fuentes and Cuillas mylonites. Fabrics reflecting a lesser degree of non-coaxiality are restricted to the central parts of the thrust units. This indicates a regional partitioning of the vorticity between the centres and the boundaries of the

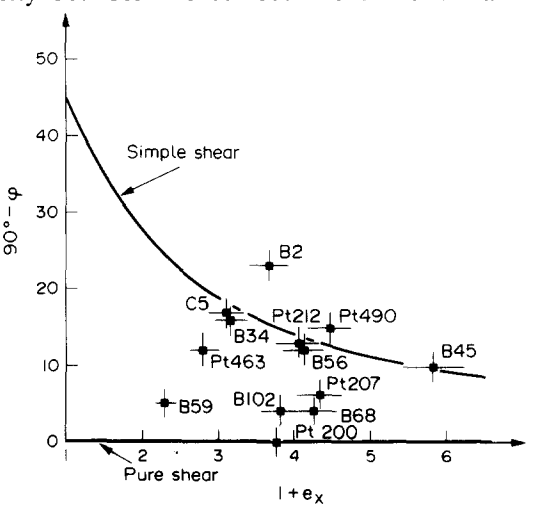

Fig. 16. Relation between the degree of external asymmetry of quartz *c*-axis fabrics (expressed by $90° - \psi$) and the finite stretch $(1 + e_x)$ along X. The angle between the XY plane and a line of zero angular velocity as a function of finite strain is plotted for progressive simple shear (curve) and progressive pure shear (along horizontal axis). The differing values of $(90° - \psi)$ indicate a wide variation in the vorticity of the flow. See text for discussion.

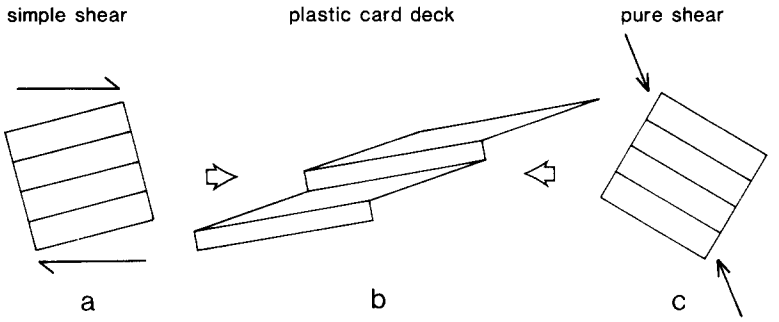

Fig. 17. Flow partitioning in a multi-layer: the plastic card-deck model. The deformed state (b), which consists of alternating domains deformed by coaxial and non-coaxial flow, can be produced by a bulk progressive simple shear (a), bulk progressive pure shear (c), or any plane-strain general non-coaxial bulk flow.

thrust units. Flow may have approximated to simple shear in and next to the Fuentes and Cuillas thrusts, whereas the interiors of the Castro Slice and the Alhamilla Unit were deformed more or less coaxially. These conclusions are broadly comparable to those of Law *et al.* (1984), who found coaxial fabrics in relatively low-strain rocks from the Moine thrust zone, and an increase in non-coaxiality towards thrust contacts. Note that regardless of the value of ψ, the fabrics do not show any features that might suggest a departure from plane strain (see Lister & Hobbs 1980); nor is there any significant variation in the extension direction indicated by either the fabric or L_s.

DISCUSSION

Why do the kinematics of flow in the BMZ depart from progressive simple shear, a history that is commonly assumed in shear-zones, even on the scale of an orogenic belt (Quinquis *et al.* 1978, Mattauer *et al.* 1981, Ramsay *et al.* 1983)? Part at least of the answer may lie in the process of flow partitioning. Zones of very high rate of deformation (and hence finite strain) such as the Fuentes and Cuillas mylonite zones can take up much of the vorticity of the bulk flow, allowing the interleaving domains to deform nearly coaxially (Lister & Williams 1983). The system can be likened to a plastic card-deck (Fig. 17) in which slip occurs on the card surfaces (the mylonite zones), while the cards themselves stretch coaxially. The kinematics of this situation have been analysed by Platt (1984).

An explanation in terms of flow partitioning leaves the nature of the bulk flow in the BMZ open, however, and this point has been emphasized in Fig. 17 by showing the development of the plastic card-deck model for both pure and simple shear deformation histories. The BMZ was undoubtedly a shear zone, in view of its tectonic position, but there is no reason to assume that the bulk flow corresponded exactly to simple shear. The overlying Aguilón nappe was undergoing significant internal deformation during emplacement (Platt *et al.* 1983), so that the compatibility constraints that restrict flow between two rigid blocks to progressive simple shear (Ramsay & Graham 1970) did not apply. In general, the upper boundaries of orogenic belts with subhorizontal nappe tectonics are unconstrained, and nappes and thrust-sheets are free to deform coaxially during emplacement. Platt *et al.* (1983) suggested that the Aguilón nappe was emplaced primarily by gravity spreading, and a similar process has been suggested for the Moine nappe by Coward (1982) and Law *et al.* (1984). This could cause a deviation in the bulk flow away from simple shear in the footwall tectonites. The widespread ocurrence in the BMZ of flow with a lower degree of non-coaxiality than simple shear should warn us not to assume that large-scale intracrustal shear-zones in active orogenic belts deform entirely by bulk simple shear.

CONCLUSIONS

The suite of distinctive structures described here, from the main-phase of isoclinal folding through to the late cataclastic event, are all spatially associated with the base of the Aguilón nappe. Similar phenomena are found beneath the Higher Betic Nappe Complex through much of the Betic Cordillera (Platt *et al.* 1984), and we suggest that they are a consequence of the displacement, possibly amounting to 50 km or more, along this contact. The characteristic features of the BMZ result from the dominance of crystal plasticity as the main deformational mechanism in quartz, succeeded by brittle deformation in the later stages, and from the associated retrograde metamorphism. These features serve to distinguish the deformation in the BMZ from the earlier events in the Nevado–Filabride Complex (which occurred under higher grade conditions and involved diffusional deformational processes that produced strongly differentiated foliations), and from the concurrent deformation in the overlying nappes (variable grade, diffusional deformation dominant).

The rocks of the BMZ were deformed under progressively decreasing temperature, from the pre-mylonite medium P/T (Barrovian) amphibolite facies metamorphism through to the low-temperature cataclastic event. This temperature drop must reflect uplift towards the Earth's surface during nappe emplacement, which is consistent with the model of Platt *et al.* (1983), involving nappe motion driven by the gravitational spreading and thinning of an orogenic welt (produced initially by plate convergence).

The asymmetric quartz fabrics in the BMZ clearly indicate the overall sense of shear, but also provide evidence for flow partitioning. This phenomenon is of considerable significance for the interpretation of fabrics and microstructures in shear zones, as it means that large volumes of rock in such zones may deform nearly coaxially, and fail to reflect the bulk sense of shear. It also warns us that we cannot assume progressive simple shear on any scale in orogenic belts.

Acknowledgements—We are grateful to José-Miguel Martínez, Bas van den Eeckhout, Eelco Janzen, Geert Konert, Ruud Weijermars and Reinoud Vissers for stimulating debates on the nature and origin of the BMZ; and to Martin Casey, Rick Law, Gordon Lister and Stefan Schmidt for discussion on fabric interpretation and the kinematics of deformation. We are indebted to Clare Pope, Andria Fowler, Richard McAvoy, Phil Jackson and the late Ron Holland for technical and secretarial help. JHB was supported during this study by a Florey European Scholarship at Queen's College, Oxford, and by Research grants from the Deutscher Akademischer Austauschdienst.

REFERENCES

Aldaya, F. 1969. Sobre el sentido de los corrimientos de los mantos Alpujarrides al Sur de la Sierra Nevada (Zona Bética, provincia de Granada). *Bol. Geol. Min. Espana* **30**, 212–217.

Andrieux, J., Fontboté, J. M. & Mattauer, M. 1971. Sur un modèle explicatif de l'arc de Gibraltar. *Bull. Soc. géol. Fr.* **7**, 115–118.

Behr, H. J. 1968. Zur tektonischen Analyse magmatischer Körper unter besonderer Berücksichtigung des Quarzkorngefüges II. *Freiberger Forsch.* **C219**, 33–98.

Behrmann, J. H. 1982. Structures and deformational processes in a zone of contact strain, beneath a nappe, Sierra Alhamilla, Spain. Unpublished D.Phil. thesis, Oxford.

Behrmann, J. H. 1984a. Patterns of palaeostress and strain beneath the Aguilón nappe, Betic Cordilleras (Spain). *Z. Dt. geol. Ges.* **135**, 293–305.

Behrmann, J. H. 1984b. A study of white mica microstructure and microchemistry in a low-grade mylonite. *J. Struct. Geol.* **6**, 283–292.

Behrmann, J. H. in press. Crystal plasticity and superplasticity in quartzite: a natural example. *Tectonophysics*.

Behrmann, J. H. & Platt, J. P. 1982. Sense of nappe emplacement from quartz c-axis fabrics; an example from the Betic Cordilleras (Spain). *Earth. Planet. Sci. Lett.* **59**, 208–215.

Bell, T. H. 1978. Progressive deformation and reorientation of fold axes in a ductile mylonite zone: the Woodroffe thrust. *Tectonophysics* **44**, 285–321.

Blacic, J. D. 1975. Plastic deformation mechanisms in quartz. The effect of water. *Tectonophysics* **27**, 271–294.

Carreras, J., Estrada, A. & White, S. 1977. The effects of folding on the *c*-axis fabrics of a quartz mylonite. *Tectonophysics* **39**, 3–24.

Coward, M. P. 1982. Surge zones in the Moine thrust zone of N.W. Scotland. *J. Struct. Geol.* **4**, 247–256.

Dewey, J. F., Pitman, W. C., Ryan, W. B. F. & Bonnin, J. 1973. Plate tectonics and the evolution of the Alpine system: *Bull. geol. Soc. Am.* **84**, 3137–3180.

Díaz de Federico, A., Gomez-Pugnaire, M. T., Puga, E. & Torres-Roldán, R. 1978. Igneous and metamorphic processes in the geotectonic evolution of the Betic Cordilleras (southern Spain). *Cuadernos Geologicos* **8**.

Didon, J., Durand-Delga, M. & Kornprobst, J. 1973. Homologies géologiques entre les deux rives du detroit de Gibraltar. *Bull. Soc. géol. Fr.* **15**, 77–104.

Egeler, C. G. & Simon, O. J. 1969. Sur la tectonique de la Zone Bétique (Cordillères Bétiques, Espagne). *Verhandelingen Kon. Ned. Akad. Wetensch.* **25**, 1–90.

García-Hernandez, M., Lopez-Garrido, A. C., Rivas, P., Sanz de Galdeano, C. & Vera, J. A. 1980. Mesozoic paleogeographic evolution of the external zones of the Betic Cordillera. *Geologie Mijnb.* **59**, 155–68.

Hermes, J. J. 1978. The stratigraphy of the Subbetic and southern Prebetic of the Velez Rubio–Caravaca area and its bearing on transcurrent faulting in the Betic Cordilleras of southern Spain. *Verhandelingen Kon. Ned. Akad. Wetensch.* **81**, 54.

Law, R. D., Knipe, R. J. & Dayan, H. 1984. Strain path partitioning within thrust sheets: microstructural and petrofabric evidence from the Moine thrust zone at Loch Eriboll, northwest Scotland. *J. Struct. Geol.* **6**, 477–498.

Lister, G. S. & Dornsiepen, U. F. 1982. Fabric transitions in the Saxony granulite terrain. *J. Struct. Geol.* **4**, 81–92.

Lister, G. S. & Hobbs, B. E. 1980. The simulation of fabric development in plastic deformation and its application to quartzite: the influence of deformation history. *J. Struct. Geol.* **2**, 355–370.

Lister, G. S. & Williams, P. F. 1979. Fabric development in shear zones: theoretical controls and observed phenomena. *J. Struct. Geol.* **1**, 283–298.

Lister, G. S. & Williams, P. F. 1983. The partitioning of deformation in flowing rock masses. *Tectonophysics* **92**, 1–33.

Lister, G. S. & Snoke, A. W. 1984. S-C Mylonites. *J. Struct. Geol.* **6**, 617–638.

Mattauer, M., Faure, M. & Malavieille, J. 1981. Transverse lineation and large-scale structures related to Alpine obduction in Corsica. *J. Struct. Geol.* **3**, 401–409.

Means, W. D., Hobbs, B. E., Lister, G. S. & Williams, P. F. 1980. Vorticity and non-coaxiality in progressive deformations. *J. Struct. Geol.* **2**, 371–378.

Nijhuis, H. J. 1964. Plurifacial Alpine metamorphism in the south-eastern Sierra de los Filabres south of Lubrin, SE Spain. Unpublished thesis, University of Amsterdam.

Paterson, M. S. & Kekulawala, K. R. S. S. 1979. The role of water in quartz deformation. *Bull. Mineral.* **102**, 92–100.

Platt, J. P. 1982. Emplacement of a fold-nappe, Betic Orogen, southern Spain. *Geology* **10**, 97–102.

Platt, J. P. 1983. Progressive refolding in ductile shear-zones. *J. Struct. Geol.* **5**, 619–622.

Platt, J. P. 1984. Secondary cleavages in ductile shear zones. *J. Struct. Geol.* **6**, 439–442.

Platt, J. P., Behrmann, J. H., Martinez, J-M. M. & Vissers, R. L. M. 1984. A zone of mylonite and related ductile deformation beneath the Alpujarride nappe complex, Betic Cordilleras, S. Spain. *Geol. Rdsch.* **73**, 773–785.

Platt, J. P. & Lister 1985. Structural evolution of a nappe complex, southern Vanoise massif, French Penninic Alps. *J. Struct. Geol.* **7**, 145–160.

Platt, J. P., van den Eeckhout, B., Janzen, E., Konert, G., Simon, O. J. & Weijermars, R. 1983. The structure and tectonic evolution of the Aguilón fold-nappe, Sierra Alhamilla, Betic Cordilleras, SE Spain. *J. Struct. Geol.* **5**, 519–538.

Platt, J. P. & Vissers, R. L. M. 1980. Extensional structures in anisotropic rocks. *J. Struct. Geol.* **2**, 387–410.

Quinquis, H., Audren, C., Brun, J. P. & Cobbold, P. R. 1978. Intense progressive shear in Ile de Groix blueschists and compatibility with subduction or obduction. *Nature, Lond.* **273**, 43–45.

Ramsay, J. G. 1967. *Folding and Fracturing of Rocks*. McGraw-Hill, New York.

Ramsay, J. G., Casey, M. & Kligfield, R. 1983. Role of shear in development of the Helvetic fold-thrust belt of Switzerland. *Geology* **11**, 439–442.

Ramsay, J. G. & Graham, R. H. 1970. Strain variation in shear belts. *Can. J. Earth Sci.* **7**, 786–813.

Sibson, R. H., Moore, J. McM. & Rankin, A. H. 1975. Seismic pumping—a hydrothermal fluid transport mechanism. *J. geol. Soc. Lond.* **131**, 653–659.

Sibson, R. H. 1980. Transient discontinuities in ductile shear zones. *J. Struct. Geol.* **2**, 165–171.

Torres-Roldán, R. 1979. The tectonic subdivision of the Betic Zone (Betic Cordilleras, southern Spain): its significance and one possible geotectonic scenario for the westernmost Alpine belt. *Am. J. Sci.* **279**, 19–51.

Vissers, R. L. M. 1981. A structural study of the central Sierra de los Filabres (Betic Zone, SE Spain), with emphasis on deformational processes and their relation to the Alpine metamorphism. *GUA Papers of Geology* Ser. 1, **15**, 1–154.

White, S. 1976. The effects of strain on the microstructures, fabrics and deformation mechanisms in quartzites. *Phil. Trans. R. Soc.* **238A**, 69–86.